

# [Rb/Zr] ratio in Ba stars as diagnostics of the companion AGB stellar mass

J. Shejeelammal<sup>1,\*</sup> & Aruna Goswami<sup>1,\*</sup>

<sup>1</sup>Indian Institute of Astrophysics, Bangalore 560034, India.

\*Corresponding author. E-mail: shejeelammal.j@iiap.res.in, aruna@iiap.res.in

MS received –; accepted –

**Abstract.** Understanding the nucleosynthesis and evolution of Asymptotic Giant Branch (AGB) stars is of primary importance as they are the main producers of some of the key elements in the Universe. They are the predominant sites for the slow neutron-capture nucleosynthesis. The exact physical conditions and nucleosynthetic processes occurring at the interior of AGB stars are not clearly understood, that hinders a better understanding of the contribution of these stars to the Galactic chemical enrichment. The extrinsic stars, which are known to have received products of AGB phase of evolution via binary mass transfer mechanisms, form vital tools to trace the AGB nucleosynthesis. The [Rb/Zr] ratio is an important diagnostic to understand the average neutron density at the s-process site and provide important clues to the mass of the companion AGB stars. In this work we have presented the estimate of [Rb/Zr] ratios, based on the high resolution spectroscopic analysis for a sample of Ba stars, and discussed how it can be used to understand the characteristics of the AGB star. Results from an analysis based on parametric model to confirm the mass of the companion AGB star are also presented.

**Keywords.** stars: Abundance—stars: chemically peculiar—stars: nucleosynthesis.

## 1. Introduction

Barium (Ba II) stars are peculiar G and K type stars which were first identified by Bidelman and Keenan (1951). Their surface chemical composition is characterized by overabundance of elements heavier than iron and  $C/O < 1$  (Barbuy et al. 1992, Allen and Barbuy 2006a, Drake and Pereira 2008, Pereira and Drake 2009). They exhibit abnormally strong lines of s-process (slow neutron-capture process) elements such as Ba II at  $\lambda$  4554 Å, Sr II at  $\lambda$  4077 Å, as well as enhanced CH, CN and  $C_2$  molecular bands. They are mostly in their Main-Sequence and giant phase of stellar evolution. Nucleosynthesis theories do not support occurrence of heavy element nucleosynthesis during the stellar evolutionary phases to which these stars belong.

It is known that the Asymptotic Giant Branch (AGB) stars are the major producers of s-process elements in the Universe (Busso et al. 1999). The s-process enriched materials produced in the interiors of the AGB stars are brought to the surface through Third Dredge-Up (TDU). The observed over abundance of heavy elements on the surface of the Ba stars could not be attributed to an intrinsic origin as they are not luminous enough to undergo s-process nucleosynthesis. This posed a challenge to the existing nucleosynthesis

theories.

The radial velocity monitoring studies of the Ba stars have shown that 85% of the Ba stars are in binaries (McClure et al. 1980, McClure 1983, 1984, McClure & Woodsworth 1990, Udry et al. 1998a,b, Lucatello et al. 2005) with a now invisible white dwarf companion. Later studies confirmed that all the giant Ba stars are binaries (Jorissen et al 2019). A generally accepted scenario that explains the observed high abundances of neutron-capture elements is a binary mass transfer picture. These stars are believed to have received via binary mass transfer mechanisms the products of the companion stars produced during their AGB phase of evolution. Hence, the chemical composition of this class of objects can be used to trace the AGB nucleosynthesis at their corresponding metallicity.

The detailed chemical composition studies of the AGB stars can help better understanding of the evolution of heavy elements in the Galaxy. The molecular contribution dominant spectra of the AGB stars make the derivation of exact elemental abundance difficult. In this regard, the spectra of the comparatively warmer, extrinsically s-process enhanced, Ba stars could make the derivation of elemental abundance much easier and help probing the s-process enrichment of the Galaxy.

Several aspects of the Ba stars such as mass, abundance peculiarities, kinematics etc. have been exten-

sively studied by many authors (Allen & Barbuy 2006a, Smiljanic et al. 2007, de Castro et al. 2016, Yang et al. 2016, Mahanta et al. 2016, Karinkuzhi et al. 2018a, Purandardas et al. 2019, Shejeelammal et al. 2020 and references therein). In addition to the probing of s-process enrichment of the Galaxy, the surface chemical composition analysis of the Ba stars could also be used to characterize the initial mass of the companion AGB stars. Mass is one of the important basic parameters of stars; the neutron source and nucleosynthesis product distribution varies with initial stellar mass. In case of AGB stars, there are two important neutron sources for the s-process in the He intershell:  $^{13}\text{C}(\alpha, n)^{16}\text{O}$  reaction during the radiative inter-pulse period and  $^{22}\text{Ne}(\alpha, n)^{25}\text{Mg}$  reaction during the convective thermal pulses.  $^{13}\text{C}(\alpha, n)^{16}\text{O}$  reaction is the dominant neutron source in low-mass AGB stars with initial mass  $\leq 3 M_{\odot}$ . The temperature required for the operation of this reaction is  $T \geq 90 \times 10^6$  K and provides a neutron density  $N_n \sim 10^8 \text{ cm}^{-3}$  in a timescale of  $\geq 10^3$  years (Straniero et al. 1995, Gallino et al. 1998, Goriely & Mowlavi 2000, Busso et al. 2001). The temperature required for the activation of  $^{22}\text{Ne}$  source is  $300 \times 10^6$  K, which is achieved during the TPs in intermediate mass AGB stars (initial mass  $\geq 4 M_{\odot}$ ). It produces a neutron density  $N_n \sim 10^{13} \text{ cm}^{-3}$  in a timescale of  $\sim 10$  years. The temperature required for the  $^{22}\text{Ne}$  source is reached in low-mass stars during the last few TPs providing  $N_n \sim 10^{10} - 10^{11} \text{ cm}^{-3}$  (Iben 1975, Busso et al. 2001).

Rb plays a unique role as diagnostics of the neutron density at the s-process site. Rb is the only low neutron density branch available to the stellar spectroscopists as a neutron densitometer (Tomkin & Lambert 1999). Rb is produced only when the  $N_n > 5 \times 10^8 \text{ cm}^{-3}$ , otherwise Sr, Y, Zr etc. are produced. Hence,  $[\text{Rb}/\text{Zr}]$  ratio can be used as an indicator of mass of AGB stars. Theoretical models predict a negative value for  $[\text{Rb}/\text{Zr}]$  ratio in low-mass AGB stars and a positive value in intermediate-mass AGB stars (Abia et al. 2001, van Raai et al. 2012, Karakas et al. 2012). We have used the neutron density dependent  $[\text{Rb}/\text{Zr}]$  ratio in a sample of barium stars to infer the mass of companion AGB stars. Such studies in literature are scanty.

In this work, we present results obtained from a detailed chemical composition analysis of four Ba stars: HD 32712, HD 36650, HD 179832 and HD 211173, based on high-resolution, high quality spectra. We have determined the abundances of heavy elements such as Rb, Sr, Y, Zr, Ba, La, Ce, Pr, Nd, Sm and Eu in these stars. The details of the spectra, abundance analysis and the interpretations of the results are discussed in the subsequent sections.

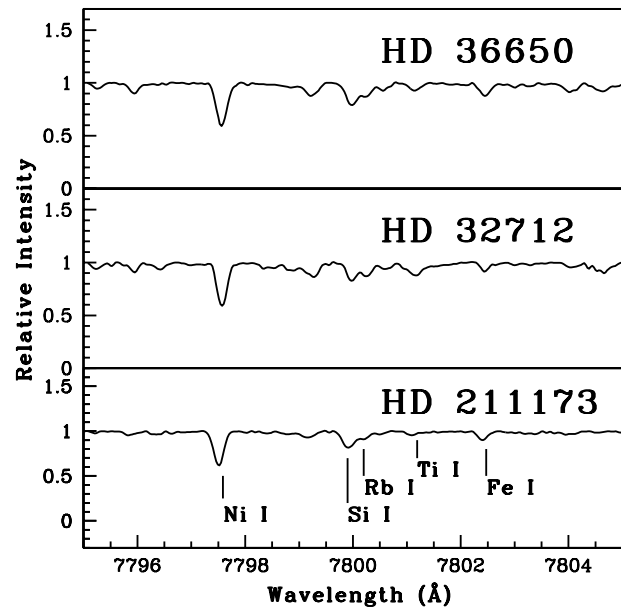


**Figure 1.** Sample spectra of the program stars in the wavelength region 7795 to 7805 Å.

## 2. Data acquisition and data reduction

The objects analysed in this study are taken from the barium star catalog of Lü (1991). The high resolution ( $\lambda/\delta\lambda \sim 48,000$ ) FEROS (Fiber-fed Extended Range Optical Spectrograph attached to the 1.52 m telescope of ESO at La Silla, Chile) spectra are used for all the four objects. The wavelength coverage spans from 3520 - 9200 Å. The data reduction is performed using the basic tasks in Image Reduction and Analysis Facility (IRAF) software. A few sample spectra are shown in Figure 1.

## 3. Data analysis

### 3.1 Determination of stellar atmospheric parameters

The data analysis is performed using the most recent version of the radiative transfer code MOOG (Snedden 1973) based on the assumptions of Local Thermodynamic Equilibrium (LTE). The stellar atmospheric parameters, the effective temperature  $T_{\text{eff}}$ , the surface gravity  $\log g$ , micro-turbulent velocity  $\zeta$ , and the metallicity  $[\text{Fe}/\text{H}]$  are determined using a set of clean, unblended Fe I and Fe II lines with excitation potential in the range 0.0 - 6.0 eV and equivalent width 20 - 180 mÅ. An initial model atmosphere is selected from the Kurucz grid of model atmosphere with no convective overshooting (<http://cfaku5.cfa.harvard.edu/>) using the photometric temperature estimate and the ini-

tial guess of  $\log g$  value for giants/dwarfs. The final model atmosphere is obtained through an iterative method from the initially selected one. The effective temperature is determined by forcing the slope of abundances versus the excitation potential of the measured Fe I lines to zero. The micro-turbulent velocity at that particular temperature is fixed to be that value for which there is no dependence of the abundances derived from the Fe I lines on the reduced equivalent width. The surface gravity is obtained by demanding the abundances derived from both Fe I and Fe II lines give nearly same values at the selected effective temperature and micro-turbulent velocity. The abundances obtained from the Fe I and Fe II lines give the metallicity. With this finally adopted model atmosphere, the further abundance analysis is carried out.

### 3.2 Abundances of heavy elements

The abundance of Rb is derived using the spectral synthesis calculation of Rb I resonance line at 7800.259 Å (Figure 2). We could not detect the Rb I lines in the warmer program stars. The Rb I resonance line at 7947.597 Å is not usable for the abundance estimation. The hyper-fine components of Rb is taken from Lambert & Luck (1976). The Sr abundance is derived from the spectral synthesis calculation of Sr I line at 4607.327 Å. The Y I line at 6435.004 Å is used to derive the Y I abundances while Y II abundances are derived from the measured equivalent width of several Y II lines. We have derived the Zr abundance from the spectral synthesis of Zr I line at 6134.585 Å (Figure 3) and from the equivalent width measurement of several Zr II lines. The abundances of Ba and La are derived from the spectral synthesis calculation of Ba II line at 5853.668 Å and La II line at 4921.776 Å. The hyper-fine components of Ba are taken from McWilliam (1998) and La from Jonsell et al. (2006). To derive the abundances of elements Ce, Pr, Nd, Sm, equivalent width measurement of several singly ionized lines are used. The Eu abundances are derived from the spectral synthesis calculation of Eu II line at 6645.064 Å by considering the hyper-fine components from Worely et al. (2013).

## 4. Results and Discussion

### 4.1 [Rb/Zr] ratio as a diagnostic of the neutron density at the s-process site

Rb is an s-process element produced from the neutron capture of  $^{84}\text{Kr}$ . The s-process path going through Rb is shown in Figure 4. The branching points at the unstable nuclei  $^{85}\text{Kr}$  and  $^{86}\text{Rb}$  controls the Rb produc-

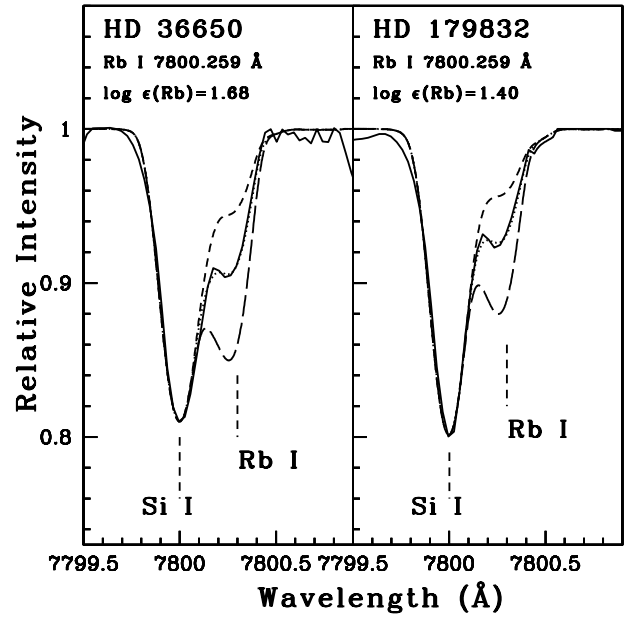


**Figure 2.** Synthesis of Rb I line around 7800 Å. Dotted line represents synthesized spectra and the solid line indicates the observed spectra. Short dashed line represents the synthetic spectra corresponding to  $\Delta[\text{Rb}/\text{Fe}] = -0.3$  and long dashed line is corresponding to  $\Delta[\text{Rb}/\text{Fe}] = +0.3$

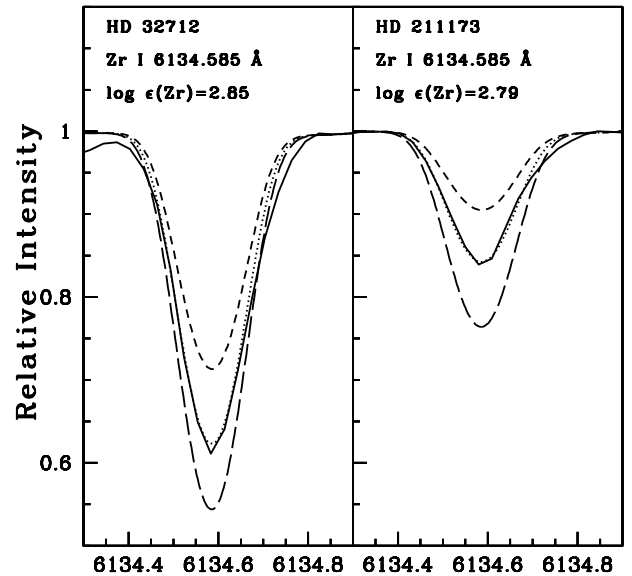
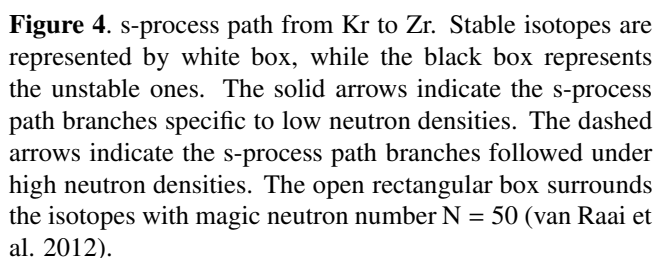


**Figure 3.** Synthesis of Zr I line at 6134.585 Å. Dotted line represents synthesized spectra and the solid line indicates the observed spectra. Short dashed line represents the synthetic spectra corresponding to  $\Delta[\text{Zr}/\text{Fe}] = -0.3$  and long dashed line is corresponding to  $\Delta[\text{Zr}/\text{Fe}] = +0.3$



Star name	[Fe/H]	[Rb/Fe] ( $\pm 0.20$ dex)	[Zr/Fe] ( $\pm 0.20$ dex)	[Rb/Zr] ( $\pm 0.20$ dex)
HD 32712	$-0.25 \pm 0.12$	$-1.13$	0.52	$-1.65$
HD 36650	$-0.02 \pm 0.12$	$-0.82$	0.51	$-1.33$
HD 179832	$+0.23 \pm 0.04$	$-1.35$	1.29	$-2.64$
HD 211173	$-0.17 \pm 0.10$	$-1.00$	0.38	$-1.38$

AGB star. But, it is impossible to distinguish the lines due to these two isotopes of Rb in the stellar spectra (Lambert & Luck 1976, García-Hernández et al. 2006). However, the abundance of Rb relative to other elements in this region of the s-process path, such as Sr, Y, and Zr, can be used to estimate the average neutron density of the s-process. Both the theoretical models and the observations have shown that the  $[\text{Rb}/\text{Zr}]$  has a negative value in AGB stars with  $M < 3M_{\odot}$  and a positive value in massive AGB stars with mass  $M > 3M_{\odot}$  (Karakas et al. 2012, Plez et al. 1993, Lambert et al. 1995, Abia et al. 2001, García-Hernández et al. 2006, 2007, 2009, van Raai et al. 2012).

We could derive the  $[\text{Rb}/\text{Zr}]$  ratio in all the four Ba stars, the estimated values are given in Table 1. The observed  $[\text{Rb}/\text{Fe}]$  and  $[\text{Zr}/\text{Fe}]$  ratios are shown in Figure 5. The observed ranges of Rb and Zr in low- and intermediate-mass AGB stars (shaded regions) in the Galaxy and Magellanic Clouds are also shown for a comparison. The comparison shows clear evidence of consistency between observed abundances of Rb and Zr in the Ba stars and their counterparts normally observed in the low-mass AGB stars. The negative values of  $[\text{Rb}/\text{Zr}]$  ratio obtained in the program stars confirm the low-mass companion for these stars.

#### 4.2 Comparison with FRUITY models and a parametric model based analysis

The observed abundance in the atmosphere of the Ba stars might not be the actual signature of the progenitor AGB stars. The accreted s-rich material is mixed and diluted in the envelope of these secondary Ba stars. The diluted theoretical abundance on the surface of Ba stars is given as (Husti et al. 2009);

$$[X/Fe] = \log(10^{[X/Fe]_{ini}} \cdot f + 10^{[X/Fe]_{AGB}} \cdot 10^{-d})$$

where  $d$  is the dilution factor,  $f = 1 - 10^{-d}$  and  $[X/Fe]^{AGB}$  is the abundance of element  $X$  in the AGB. In this formulation it is assumed that both the AGB and the Ba stars are formed from the same cloud of interstellar medium (Husti et al. 2009).

We have performed a parametric model based analysis in order to confirm the mass of the companion AGB stars by incorporating the dilution experienced by the s-rich material after the mass transfer. The dilution

tion along the s-process nucleosynthesis path through Rb. The probability of these unstable nuclei to capture the neutron before  $\beta$ -decaying determines the amount of Rb produced, which in turn depends on the neutron density at the s-process site (Beer & Macklin 1989, Tomkin & Lambert 1983, Lambert et al. 1995). When  $^{84}\text{Kr}$  undergoes neutron capture, 50% of the flux goes to the ground state of  $^{85}\text{Kr}$  and other 50% goes to the metastable state of  $^{85}\text{Kr}$ . Out of this metastable  $^{85}\text{Kr}$ , 80% decays to  $^{85}\text{Rb}$ , while the remaining 20% decays to its ground state. In effect, 40% of the  $^{84}\text{Kr}+n$  produces  $^{85}\text{Rb}$ , whereas the remaining 60% results in the production of ground state  $^{85}\text{Kr}$ . At higher neutron densities,  $N_n > 5 \times 10^8 \text{ n/cm}^3$ , the long-lived  $^{85}\text{Kr}$  ( $t_{1/2} \sim 10.75 \text{ yrs}$ ) undergo neutron capture allowing the reaction  $^{85}\text{Kr}(n, \gamma)^{86}\text{Kr}(n, \gamma)^{87}\text{Kr}$ . The short-lived  $^{87}\text{Kr}$  ( $t_{1/2} \sim 76.3 \text{ min}$ ) decays quickly to the stable  $^{87}\text{Rb}$ . The other unstable isotope  $^{86}\text{Rb}$  ( $t_{1/2} \sim 18.63 \text{ days}$ ), which is produced by the neutron capture of  $^{85}\text{Rb}$ , directly produces  $^{87}\text{Rb}$  provided the neutron density is  $\geq 10^{10} \text{ n/cm}^3$ . At lower neutron densities,  $^{86}\text{Rb}$  decays to  $^{86}\text{Sr}$  allowing for  $^{86}\text{Sr}(n, \gamma)^{87}\text{Sr}(n, \gamma)^{88}\text{Sr}$  (Beer 1991, Lugaro & Chieffi 2011).

The magic number of neutrons of  $^{87}\text{Rb}$  makes it stable against neutron capture. The smaller neutron-capture cross-section of  $^{87}\text{Rb}$  ( $\sigma \sim 15.7$  mbarn at 30 KeV) compared to that of  $^{85}\text{Rb}$  ( $\sigma \sim 234$  mbarn) (Heil et al. 2008a) favours the accumulation of  $^{87}\text{Rb}$  once it is formed. Therefore, the isotopic ratio  $^{87}\text{Rb}/^{85}\text{Rb}$  could be a direct indicator of the neutron density at the s-process site, which in turn help to infer the mass of the

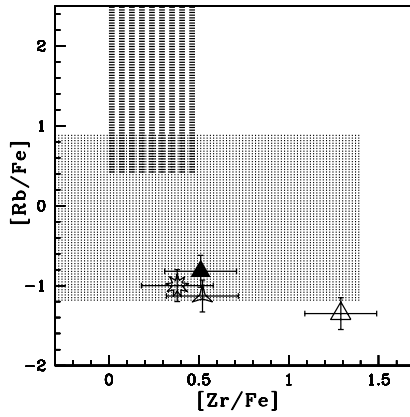


**Figure 5.** The observed abundances  $[Rb/Fe]$  vs  $[Zr/Fe]$ . HD 32712 (starred triangle), HD 36650 (filled triangle), HD 179832 (open triangle), and HD 211173 (nine-sided star). The region shaded with short-dashed line and dots corresponds to the observed range of Zr and Rb in intermediate-mass and low-mass AGB stars respectively in the Galaxy and the Magellanic Clouds (van Raai et al. 2012).

factor,  $d$ , is defined as  $M_{\star}^{env}/M_{AGB}^{transf} = 10^d$ , where  $M_{\star}^{env}$  is the mass of the envelope of the observed star after the mass transfer,  $M_{AGB}^{transf}$  is the mass transferred from the AGB. The dilution factor is derived by comparing the observed abundance with the predicted abundance from FRUITY model for the heavy elements (Rb, Sr, Y, Zr, Ba, La, Ce, Pr, Nd, Sm and Eu). A publicly available (<http://fruity.oa-teramo.inaf.it/>, Web sites of the Teramo Observatory (INAF)) data set for the s-process in AGB stars is the FRANEC Repository of Updated Isotopic Tables & Yields (FRUITY) models (Cristallo et al. 2009, 2011, 2015b). These models cover the whole range of metallicity observed for Ba stars from  $z = 0.001$  to  $z = 0.020$  for the mass range  $1.3 - 6.0 M_{\odot}$ . We have compared our estimated abundances with the FRUITY model. The solar values are taken as the initial composition. The observed elemental abundances are fitted with the parametric model function. The best fitting masses and corresponding dilution factors along with the  $\chi^2$  values are given in Table 2. A few examples of the best fits obtained are shown in Figure 6. All the Ba stars are found to have low-mass AGB companions with  $M \leq 3 M_{\odot}$ .

In the FRUITY models, a standard  $^{13}C$  pocket is being considered, the different  $^{13}C$  pocket efficiencies may explain the observed discrepancy. Also, inclusion of stellar rotations may cause the deviation in the observed abundance pattern, which is lacking in the current FRUITY models. Rotation induced mixing is found to alter the extend of  $^{13}C$  pocket, altering the s-process abundance pattern (Langer et al. 1999). However, we note that, a study made by Cseh et al. (2018)

**Table 2.** The best fitting mass, dilution factor and reduced chi-square values.

star name	$M_{AGB}$ ( $M_{\odot}$ )	$d$	$\chi^2$
HD 32712	2.0	0.001	16.14
HD 36650	3.0	0.04	8.08
HD 179832	3.0	0.75	48.01
HD 211173	2.5	0.03	18.15

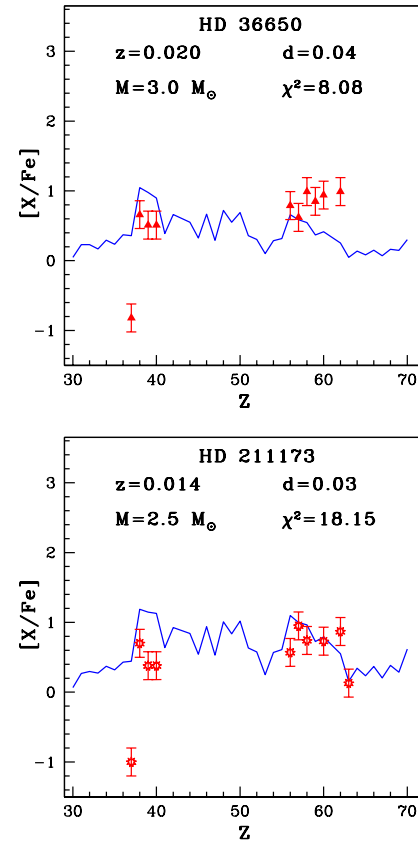


**Figure 6.** Solid curve represent the best fit for the parametric model function. The points with error bars indicate the observed abundances in the program stars.

using the rotating star models available for the metallicity range of Ba stars (Piersanti et al. 2013) could not reproduce the observed abundance ratios of stars studied in de Castro et al. (2016).

#### 4.3 The $[hs/ls]$ ratio

In addition to the  $[Rb/Zr]$  ratio, the  $[hs/ls]$  ratio in the Ba stars is an indicator of the neutron source and hence the mass of the AGB stars. Here  $ls$  refers to the light s-process elements (Sr, Y and Zr) and  $hs$  to the heavy s-process elements (Ba, La, Ce and Nd). The observed  $[hs/ls]$  ratio is in the range 0.19 - 1.15, which agrees with the model calculations of Busso et al. (2001) for similar metallicities, for low mass AGB stars considering  $^{13}C(\alpha, n)^{16}O$  neutron source. This also confirms the lower-mass for the companion AGBs.

#### 4.4 Comparison with low-mass AGB abundance

We have compared the observed abundance ratios for eight neutron-capture elements in the Ba stars with their counterparts in the low-mass AGB stars from literature, that are found to be associated with  $^{13}C(\alpha, n)^{16}O$  neutron source (Figure 7). The comparison shows a pretty good match between the abundances observed in both Ba stars and the AGBs. The scatter observed in the ratios may be a consequence of different dilution factors during the mass transfer, as well as the orbital parameters, metallicity and initial mass (de Castro et al. 2016).

#### 4.5 Mg abundance in support of neutron source.

Another check for the companion AGB mass is the Mg abundance. A Mg enrichment is expected to observe in the stars if the s-process over abundance is resulting from the neutrons produced during the convective thermal pulses through the reaction  $^{22}Ne(\alpha, n)^{25}Mg$ . A comparison of the Mg abundances observed in the program stars and that in the disk stars and field giants is illustrated in Figure 8. As it is obvious from the figure, we could not find any enhancement of Mg in our sample when compared to the disk stars and normal giants. This discards the fact that the origin of neutron is  $^{22}Ne(\alpha, n)^{25}Mg$  source.

### 5. Conclusion

The detection of Rb I line at 7800.259 Å in the spectra of four program stars allowed us to determine  $[Rb/Zr]$  ratio for these objects. The negative values obtained for this ratio in these stars indicate the operation of  $^{13}C(\alpha, n)^{16}O$  reaction. As this reaction occurs in the low-mass AGB stars, we confirm that the former com-

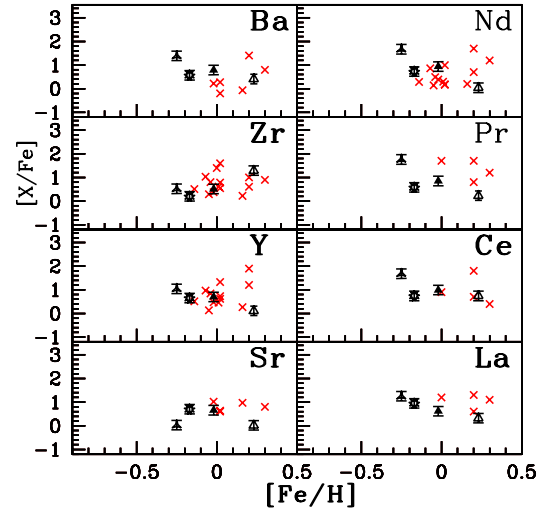


**Figure 7.** Comparison of abundance ratios of neutron-capture elements observed in the program stars and the AGB stars with respect to metallicity  $[Fe/H]$ . Red crosses represent the AGB stars from literature (Smith & Lambert 1985, 1986b, 1990, Abia & wallerstein 1998). HD 32712 (starred triangle), HD 36650 (filled triangle), HD 179832 (open triangle) and HD 211173 (nine-sided star).

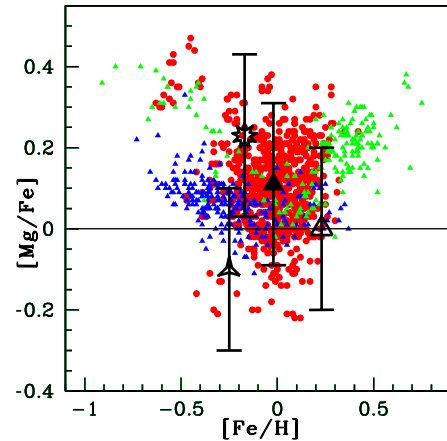


**Figure 8.** Abundances of Mg in our program stars, HD 32712 (starred triangle), HD 36650 (filled triangle), HD 179832 (open triangle) and HD 211173 (nine-sided star) compared with the disk dwarfs and field giants. Red circles represent normal field giants from literature (Luck & Heiter, 2007). Blue triangles represent thin disk dwarfs from Bensby et al. (2004), Reddy et al. (2003). Green triangles represent thick disk dwarfs from Bensby et al. (2004), Reddy et al. (2006).

panions of these stars are low-mass AGB stars with  $M \leq 3 M_{\odot}$ . A comparison of observed abundances with the predictions from FRUITY models, and with those that are observed in low-mass AGB stars from literature, also confirms low-mass for the former companion AGB stars. The observed  $[\text{hs}/\text{ls}]$  ratio in the range 0.19 - 1.15, that agrees with the model calculations of Busso et al. (2001) for AGB stars considering  $^{13}\text{C}(\alpha, n)^{16}\text{O}$  neutron source, is also an indication of low-mass for the companion AGBs. An enhancement of Mg abundances compared to their counterparts in disk stars and normal giants would have indicated the operation of  $^{22}\text{Ne}(\alpha, n)^{25}\text{Mg}$ . We did not find any enhancement of Mg in our sample and hence discard the source of neutron as the  $^{22}\text{Ne}(\alpha, n)^{25}\text{Mg}$  reaction. This again confirms low-mass for the companion AGBs.

## Acknowledgements

Funding from the DST SERB project No. EMR/2016/005283 is gratefully acknowledged. This work made use of the SIMBAD astronomical database, operated at CDS, Strasbourg, France, and the NASA ADS, USA. This work has made use of data from the European Space Agency (ESA) mission Gaia (<https://www.cosmos.esa.int/gaia>), processed by the Gaia Data Processing and Analysis Consortium (DPAC), <https://www.cosmos.esa.int/web/gaia/dpac/consortium>).

## References

- Abia C., Wallerstein G., 1998, MNRAS, 293, 89
- Abia C., Busso M., Gallino R., Domínguez I., Straniero O. & Isern J., 2001, ApJ, 559, 1117
- Allen D.M., Barbuy B., 2006a, A&A, 454, 895
- Barbuy B., Jorissen A., Rossi S. C. F. & Arnould M., 1992, A&A, 262, 216
- Beer H., 1991, ApJ, 375, 823
- Beer H. & Macklin R. L., 1989, ApJ, 339, 962
- Bensby T., Feltzing S., Lundstrom I., 2004, A&A, 415, 155
- Bidelman W.P., Keenan P.C., 1951, ApJ, 114, 473
- Busso M., Gallino R., Wasserburg G. J., 1999, ARA&A, 37, 239
- Busso M., Gallino R., Lambert D. L., Travaglio C., Smith V. V., 2001, ApJ, 557, 802
- Cristallo S., Straniero O., Gallino R., Piersanti L., Domínguez I., Lederer M. T., 2009, ApJ, 696, 797
- Cristallo S., Piersanti L., Straniero O., Gallino R., Domínguez I., Abia C., di rico G., Quintini M., Bisterzo S., 2011, ApJS, 197, 17
- Cristallo S., Straniero O., Piersanti L. & Gobrecht D., 2015b, ApJS, 219, 40
- Cseh B., Lugaro M., D’Orazi V., de Castro D. B., Pereira C.B., Karakas A. I. et al., 2018, A&A, 620, A146
- de Castro D.B., Pereira C.B., Roig F., Jilinski E., Drake N.A., Chavero C., Sales Silva J.V., 2016, MNRAS, 459, 4299
- Drake N. A. & Pereira C. B., 2008, AJ, 135, 1070
- Gallino R., Arlandini C., Busso M., Lugaro M., Travaglio C., Straniero O., Chieffi A., Limongi M., 1998, ApJ, 497, 388
- García-Herández D. A., García-Lario P., Plez B., D’Antona F., Manchado A., Trigo-Rodríguez M., 2006, Science, 314, 1751
- García-Herández D. A., García-Lario P., Plez B., Manchado A., D’Antona F., Lub J. & Habing H., 2007, A&A, 462, 711
- García-Herández D. A., Manchado A., Lambert D. L., Plez B., García-Lario P., D’Antona F., Lugaro M., Karakas A. I. & van Raai M. A., 2009, ApJ, 705, L31
- Goriely S., Mowlavi N., 2000, A&A, 362, 599
- Heil M., Käppeler F., Uberseder E., Gallino R., bisterzo S., Pignatari M., 2008a, Phys. Rev. C, 78, 5802
- Husti L., Gallino R., Bisterzo S., Straniero O. & Cristallo S., 2009, PASA, 26, 176
- Iben Jr. I., 1975, ApJ, 196, 525
- Jonsell K., Barklem P. S., Gustafsson B., Christlieb N., Hill V., Beers T. C., Holmberg J., 2006, A&A, 451, 651
- Jorissen A., Boffin H. M. J., Karinkuzhi D., Van Eck S., Escorza A. et al., 2019, A&A, 626A, 127J
- Karakas A.I., García-Hernández D. A. & Lugaro M., 2012, ApJ, 751, 8
- Karinkuzhi D., Goswami A., Sridhar N., Masseron T., Purandaras M., 2018a, MNRAS, 476, 3086K
- Lambert D. L. & Luck R. E., 1976, Obs., 96, 100L
- Lambert D. L., Smith V. V., Busso M., Gallino R. & Straniero O., 1995, ApJ, 450, 302
- Langer N., Heger A., Wellstein S. & Herwig F., 1999, A&A, 346, L37
- Lü P.K., 1991, AJ, 101, 2229
- Lucatello S., Tsangarides S., Beers T. C., Carretta E., Gratton R. G., Ryan S. G., 2005, ApJ, 652, 825
- Luck R. E. & Heiter U., 2007, AJ, 133, 2464
- Lugaro M. & Chieffi A., 2011, in Lecture Notes in Physics, ed. R. Diehl, D. H. Hartmann & N. Prantzos (Berlin: Springer Verlag), 812, 83



- Mahanta U., Karinkuzhi D., Goswami A., Duorah K., 2016, MNRAS, 463, 1213
- McClure R.D., 1983, ApJ, 208, 264
- McClure R.D., 1984, ApJ, 280, 31
- McClure R.D., Woodsworth W., 1990, ApJ, 352, 709
- McClure R. D., Fletcher J. M., Nemec J., 1980, ApJ, 238, L35
- McWilliam A., 1998, AJ, 115, 1640
- Pereira C. B., Drake N. A., 2009, A&A, 496, 791
- Piersanti L., Cristallo S. & Straniero O., 2013, ApJ, 774, 98
- Plez B., Smith V. V. & Lambert D. L., 1993, ApJ, 418, 812
- Purandardas M., Goswami A., Goswami P. P., Shejeelammal J., Masseron T., 2019, MNRAS, 486, 3266
- Reddy B.E., Tomkin J., Lambert D.L. & Allende Prieto C., 2003, MNRAS, 340, 304
- Reddy B.E., Lambert D.L., Prieto C.A., 2006, MNRAS, 367, 1329
- J. Shejeelammal, Goswami A., Goswami P. P., Rathour R. S., Masseron T., 2020, MNRAS, 492, 3708
- Smiljanic R., Porto de Mello G. F., da Silva L., 2007, A&A, 468, 679
- Smith V. V., Lambert D. L., 1985, ApJ, 294, 326
- Smith V. V., Lambert D. L., 1986b, ApJ, 311, 843
- Smith V. V., Lambert D. L., 1990, ApJS, 72, 387
- Snedden C., 1973, PhD thesis, Univ. Texas
- Straniero O., Gallino R., Busso M., Chiefei A., Raiteri C. M., Limongi M., Salaris M., 1995, ApJ, 440, L85
- Tomkin J. & Lambert D. L., 1983, ApJ, 273, 722
- Tomkin J. & Lambert D. L., 1999, ApJ, 523, 234
- Udry S., Jorissen A., Mayor M., Van Eck S., 1998a, A&AS, 131, 25
- Udry S., Mayor M., Van Eck S., Jorissen A., Prévot L., Grenier S., Lindgren H., 1998b, A&AS, 131, 43
- van Raai M. A., Lugaro M., Karakas A. I., García-Hernández D. A. & Yong D., 2012, A&A, 540, A44
- Worely C.C., Hill V. J., Sobeck J., Carretta E., 2013, A&A, 553, A47
- Yang G.C., Liang Y.C., Spite M., Chen Y.Q., Zhao G. et al., 2016, RAA, 16, 1